Psoriasis-like inflammation induces mitochondrial function and structure changes in human keratinocytes and fibroblasts

Gabrielė Kulkovienė[1,2*], Martyna Uldukytė[2], Sofiya Haluts[1], Milda Kairytė[3], Jonas Šoliūnas[1], Viktorija Šalčiūtė[2], Ramunė Morkūnienė[1], Aistė Jekabsone[2,3**]

[1] Department of Drug Chemistry, Faculty of Pharmacy, Lithuanian University of Health Sciences, 50166, Kaunas, Lithuania,

[2] Laboratory of Pharmaceutical Sciences Institute of Pharmaceutical Technologies, Lithuanian University of Health Sciences, 50166, Kaunas, Lithuania.

[3] Preclinical Research Laboratory for Medicinal Products Institute of Cardiology, Lithuanian University of Health Sciences, 50166, Kaunas, Lithuania

* Correspondence: gabriele.kulkoviene@lsmu.lt

** Correspondence: aiste.jekabsone@lsmu.lt

Keywords: mitochondria, psoriasis, inflammation, cristae, STED nanoscopy.

Conflict of Interest Statement

The authors declare no conflicts of interest.

Abstract

Mitochondrial structural and functional changes accompany psoriasis; however, the mitochondrial response to psoriatic inflammation in keratinocytes and fibroblasts has not been studied. Here, we investigate the effect of psoriasis-like inflammation (PLI) induced by cytokine cocktail (IL-17, IL-22, TNF-α) on mitochondrial network morphology and function in living cultured keratinocytes (HaCaT) and fibroblasts (BJ-5ta). In both skin cell types, PLI triggered expression of psoriasis-related SKALP/Elafin and high amounts of cytokines (IL-1, IL-6), interferons (IFN-α, IFN-β, IFN-γ), and chemokines (CCL5, CXCL8), accompanied by mitochondrial ROS production, network fragmentation, swelling, and cristae disassembly. STED nanoscopy revealed that the mitochondrial cristae are disappearing in response to PLI, with the process starting faster and being more pronounced in keratinocytes than in fibroblasts. Moreover, in keratinocytes, PLI leads to mitochondrial respiration suppression and elimination of the organelles. These findings of cell-specific mitochondrial responses may guide future investigations into new pharmacological targets for managing psoriasis.

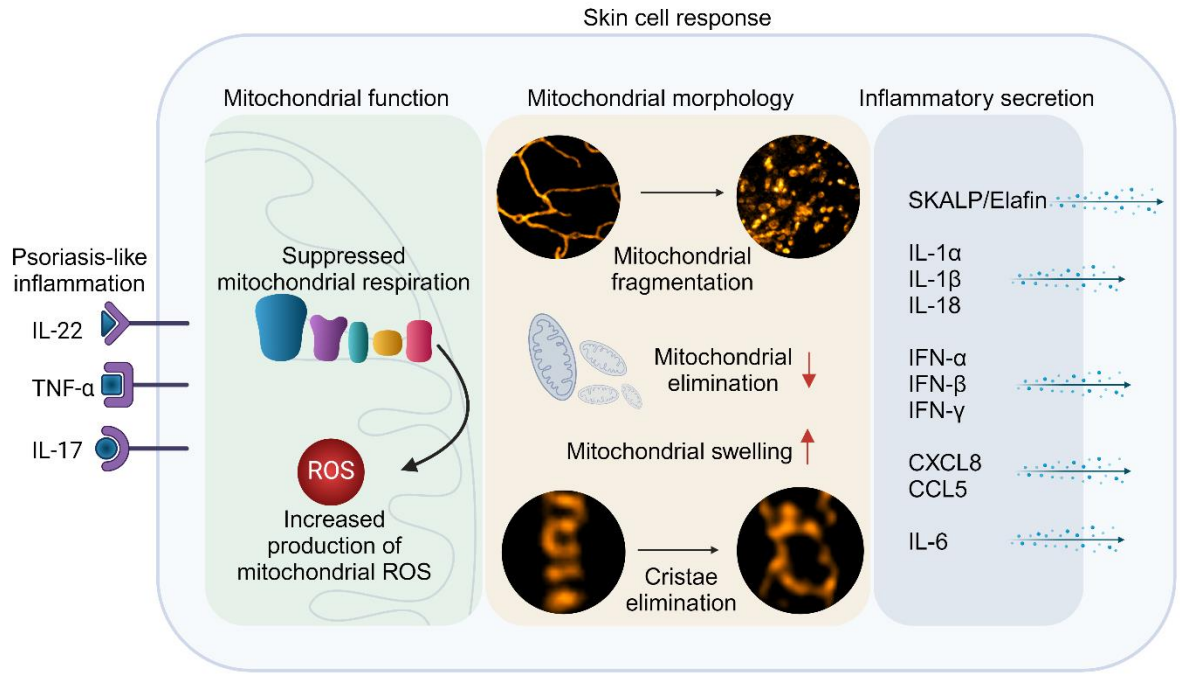

Introduction

Psoriasis is a chronic recurrent inflammatory skin disease characterized by immune system dysregulation and epidermal hyperproliferation. During psoriasis, immune cell-derived pro-inflammatory cytokines affect keratinocytes and fibroblasts, resulting in psoriatic inflammation, which promotes the formation of lesions [1]. A cytokine cocktail comprising tumor necrosis factor (TNF)-α, interleukin (IL)-17A, and IL-22 can mimic psoriasis-like inflammation (PLI) *in vitro* [2], [3]. PLI increases the production of antimicrobial peptides (SKALP/Elafin, β-defensin, LL-37), which act as potential autoantigens for immune cells at early disease stage [4]. For instance, *PI3*, encoding SKALP/Elafin, is not expressed in the normal human epidermis [5], and the secretion of this protein is linked with disease severity [6].

Biological agents acting systemically on psoriasis-related cytokines are considered the most advanced treatment for psoriasis. However, biological therapies show variability in response among individuals, are expensive and can lead to severe side effects [7]. A better understanding of the disease pathogenesis would allow new, more efficient treatment strategies.

Recent evidence suggests mitochondrial involvement in psoriasis pathogenesis, with mitochondrial reactive oxygen species (MitoROS) and network organization playing a central role. *In vivo* studies revealed MitoROS-dependent dendritic cell activation, while MitoROS scavenging effectively reduced epidermal hyperplasia and infiltration of inflammatory cells [8]. Mitochondrial fragmentation in macrophages induced psoriasis-related cytokines and facilitated their movement to the epidermis [9]. However, it remains unclear if such mitochondrial dysfunction occur in keratinocytes and fibroblasts, the critical players in psoriasis pathogenesis. Understanding the role of MitoROS and mitochondrial network-

controlling factors in these cells could offer potential therapeutic targets for fighting psoriatic inflammation.

Mitochondria respond to stress through changes in their structural dynamics, with a particular role in cristae architecture [10]. Recent advances in super-resolution microscopy enabled visualization of cristae dynamics in living cells and can provide new data about the role of mitochondrial health in psoriasis.

In our study, we investigated and compared the response of the mitochondrial function, network, and cristae architecture to PLI in fibroblasts and keratinocytes. We induced PLI by a cytokine cocktail TNF-α, IL-17A, and IL-22, confirmed the model by SKALP/Elafin mRNA expression and secretion of psoriasis-related cytokines, and assessed mitochondrial function, ROS production, network and cristae structure through STED nanoscopy analysis.

Results

Induction and validation of psoriasis-like inflammation in keratinocytes and fibroblasts

After treating human skin keratinocytes (KCs) and fibroblasts (FCs) with IL-17, IL-22, and TNF-α for 24 hours to induce PLI, PrestoBlue viability assessment indicated an 11.5% decline in PL-KCs' metabolic activity and 31% in PL-FCs (Supplementary figure S1). This decline remained stable for 48 and 72 hours, indicating the model's stability for further research. The psoriatic skin marker *PI3* expression increased significantly: 5.27-fold in KCs and 7.8-fold in FCs (log2) (Figure 1a). SKALP/Elafin secretion also rose significantly: 47.98 ±18.93 pg/ml in KCs and 0.38±0.11 pg/ml in FCs (Figure 1b). In untreated controls, protein expression and secretion were near zero or undetectable. An increase in SKALP/Elafin confirms PLI-related changes in KCs and FCs; therefore, we refer to them as psoriatic-like (PL) cells in this study.

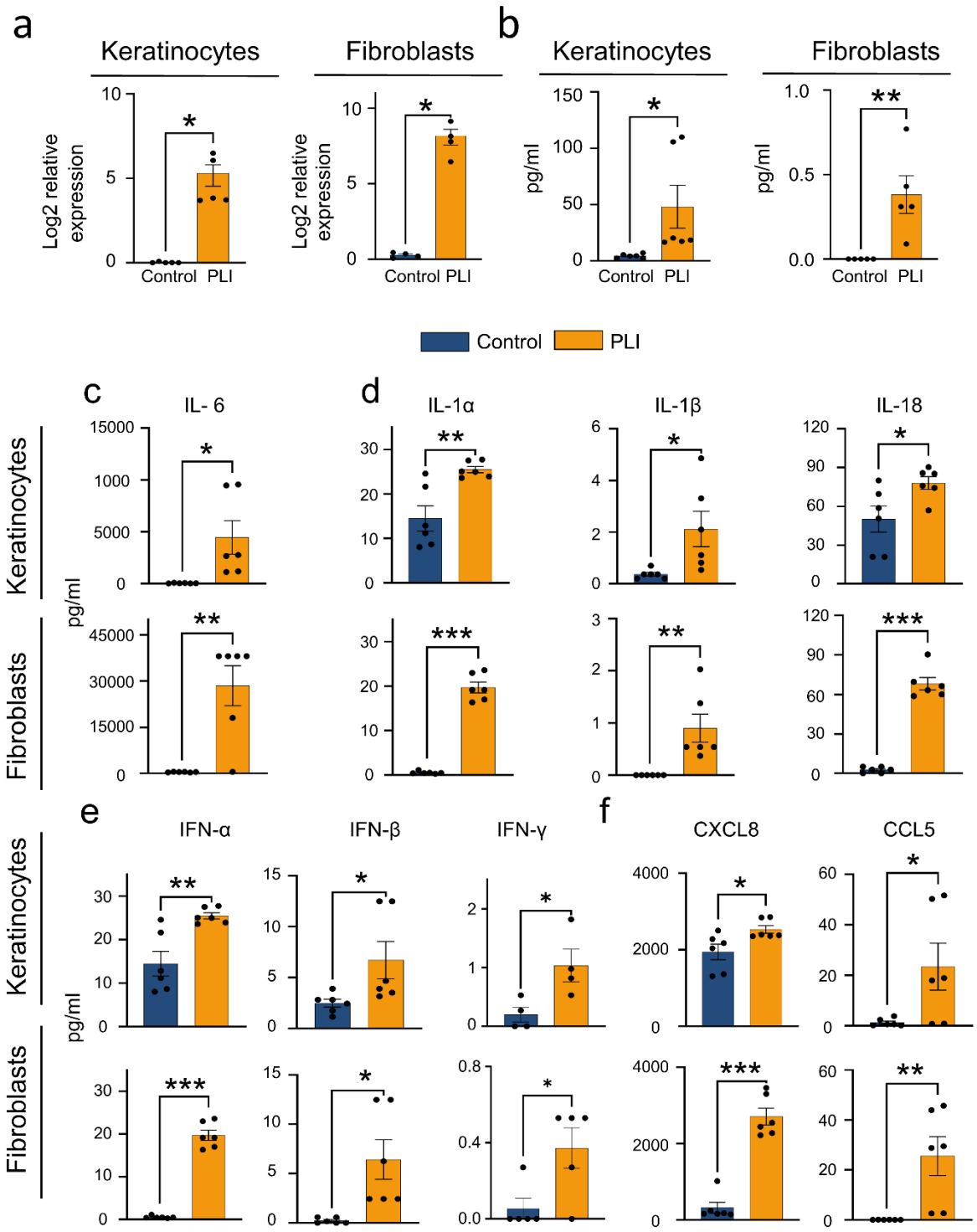

Figure 1. Induction and validation of psoriasis-like inflammation (PLI) in keratinocytes and fibroblasts

(a) *PI3* gene expression. Gene expression was evaluated by RT-qPCR; n=4-5. The fold change was expressed in Log2 form.
(b) Secretion of SKALP/Elafin.
(c) Secretion of IL-6.
(d) Secretion of IL-1 family members.

(e) Secretion of interferons IFN-α, IFN-β, IFN-γ.
(f) Secretion of chemokines CXCL8 and CCL5.
Protein levels were quantified by Luminex multiplex assay; n = 4-6. Data represented as mean±SEM. Statistically significant differences were determined by unpaired, two-tailed Student's t-test. *$p < 0.05$, ** $p < 0.01$, *** $p < 0.001$.

Under PLI conditions, both FCs and KCs secreted significantly higher amounts of IL-6 (Figure 1c), cytokines from IL-1 family (IL-1α, IL-1β, IL-18, Figure 1d), interferons (IFN-α, IFN-β, IFN-γ, Figure 1e), and chemokines (CCL5, CXCL8, Figure 1f) compared to the untreated controls. The most noticeable concentration increase in both cell types was for IL-6 (Figure 1c), a key mediator of Th17-driven cutaneous inflammation necessary for initiating psoriasis. In KCs, IL-6 rose from 0.03±0.01 ng/ml in controls to 4.40±1.60 ng/ml after PLI. In PL-FCs, the IL-6 increased from 0.40±0.03 ng/ml to 28.50±6.50 ng/ml.

In control KCs, IL-1α levels were 14.50±2.80 pg/ml, increasing to 25.48±1.70 pg/ml under PLI. For control FCs, IL-1α was measured at 0.50±0.29 pg/ml, rising to 19.70±3.00 pg/ml under PLI (Figure 1d). IL-18 and IL-1β, associated with inflammasome activation, also increased in both PL-cell types (Figure 1d). In KCs, IL-18 rose from 50.16±10.10 pg/ml to 78.11±4.92 pg/ml, while IL-1β increased from 0.36±0.18 pg/ml to 2.21±1.68 pg/ml. In FCs, IL-18 increased from 2.61±0.92 pg/ml to 68.06±4.74 pg/ml, and IL-1β from undetectable level reached 0.90±0.60 pg/ml.

IFN-α were the most elevated among the measured interferons, with concentration rising from 14.49±2.80 pg/ml to 25.48±0.72 pg/ml in KCs and from 0.52±0.11 pg/ml to 19.71±1.22 pg/ml in FCs. IFN-β rise was not as significant (from 2.40±0.38 to 6.70±1.84 pg/ml for KCs and from 0.22±0.11 to 6.42±2.00 pg/ml for FCs), and IFN-γ concentration increase was the lowest (from 0.20±0.13 to 1.04±0.27 pg/ml for KCs and from 0.05±0.05 to 0.37±0.10 pg/ml for PCs, Figure 1e).

CCL5 and CXCL8 were detected at high levels in PL cells (Figure 1f). In KCs CXCL8 increased from 1.94±0.20 to 2.50±0.10 ng/ml, and in FCs, CXCL8 rose from 0.31±0.14 to 2.70±0.21 ng/ml. CCL5 concentration increased similarly in both cell types (from 1.30±0.60 to 23.41±9.20 pg/ml in KCs, from 0.04±0.01 to 25.50±7.70 pg/ml in FCs).

While both cell types secreted higher amounts of cytokines and chemokines after PLI induction, a notable distinction emerged in their secretion profiles. PL-FCs produced higher levels of IL-6 and CXCL8 compared to PL-KCs, while PL-KCs secreted more IL-1β than PL-FCs. The results suggest that both cell types participate in PLI propagation with distinct roles.

Bioenergetic activity and MitoROS production in psoriatic-like keratinocytes and fibroblasts

The increase of pro-inflammatory mediators detected in PL cells may be related to changes in energy metabolism which is related to MitoROS production, inflammation, apoptosis, and proliferation in psoriasis. We examined mitochondrial and glycolytic activity using Seahorse XFp MitoStress assay (Figure 2a-2c) and visualized mitochondrial superoxide radicals with MitoSOX (Figure 2d-2e).

PL-KCs exhibited a significant decrease in overall mitochondrial oxygen consumption rate (OCR). Basal respiration was decreased by 40%, leading to a drop in ATP production, and maximal respiration was suppressed by 37% (Figure 2). Similarly, spare respiratory capacity in PL-KCs was 34% lower than in control (Figure 2b). In contrast, PL-FCs showed no significant changes in OCR.

The glycolytic activity was also suppressed in PL-KCs, dropping to 50% of the control cells. Again, no changes were observed in PL-FCs (Figure 2c). Overall, results suggest selective energy suppression in PL-KCs.

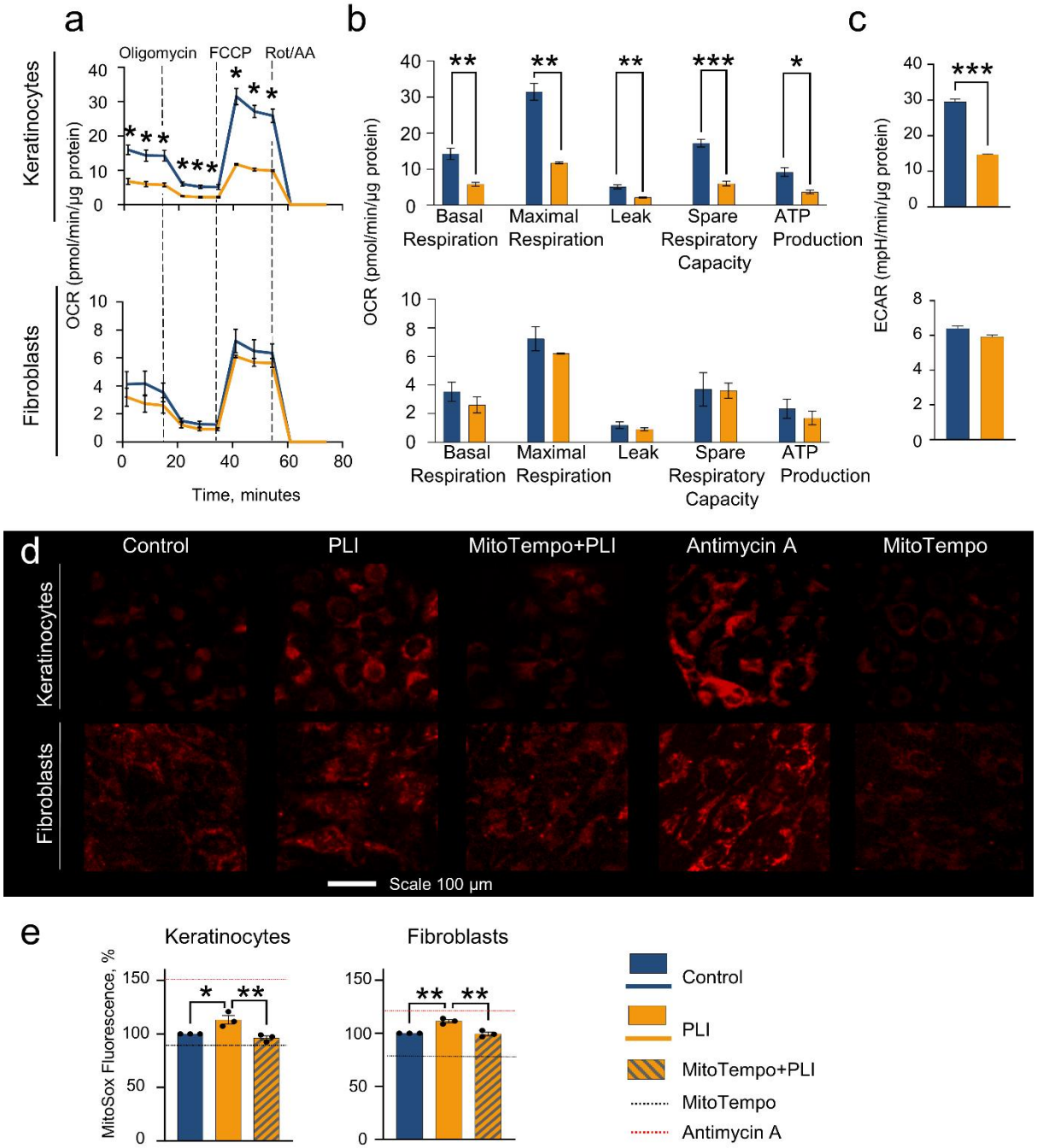

Figure 2. Psoriasis-like inflammation affects bioenergetic functionality and mitochondrial ROS of keratinocytes and fibroblasts.
(a) Representative real-time oxygen consumption rates (OCR) curves, with non-mitochondrial respiration values subtracted.
(b) Summarized OCR parameters: Basal respiration was measured at three initial points: maximal respiration – by OCR after FCCP injection and Leak – after Oligomycin injection. Spare Respiratory Capacity was calculated by subtracting basal respiration from maximal, and ATP production calculated by subtracting proton leak stimulated respiration from basal.
(c) Extracellular acidification rate (ECAR) represents glycolysis efficiency.
Statistics: Student's t-test.
(d) Fluorescent microscopy images of MitoSOX-labeled cells. Antimycin A was used as a positive control, and MitoTempo - as a negative control.
(e) Quantitative MitoSOX fluorescence results.
Statistics: one-way ANOVA Tukey's test.
Data: Mean ± SEM. *$p<0.05$, **$p<0.01$, ***$p<0.0001$, n=3

MitoROS-dependent fluorescence was higher in both PL-cell types (Figure 2d,e); increasing by 13.3% in PL-KCs and 11.4% in PL-FCs. Thus, PLI-affected KCs and FCs have elevated MitoROS production.

Psoriasis-like inflammation disrupts mitochondrial network

Recent studies suggest that mitochondrial fragmentation, due to decreased fusion and increased fission, is crucial for cytokine production in psoriasis [9]. However, data on mitochondrial network integrity in KCs and FCs under PLI is lacking. Unveiling these changes could present a potential therapeutic target.

In line with this objective, we performed mitochondrial morphometry analysis using Mito Live Orange dye, STED nanoscopy and MiNa toolset in Fiji, following the steps depicted in Supplementary Figure S2. As a positive assay control, we used the mitochondrial stressor FCCP, which makes the mitochondrial inner membrane proton-permeable, leading to membrane potential loss and mitochondrial fragmentation [11], [12], [13].

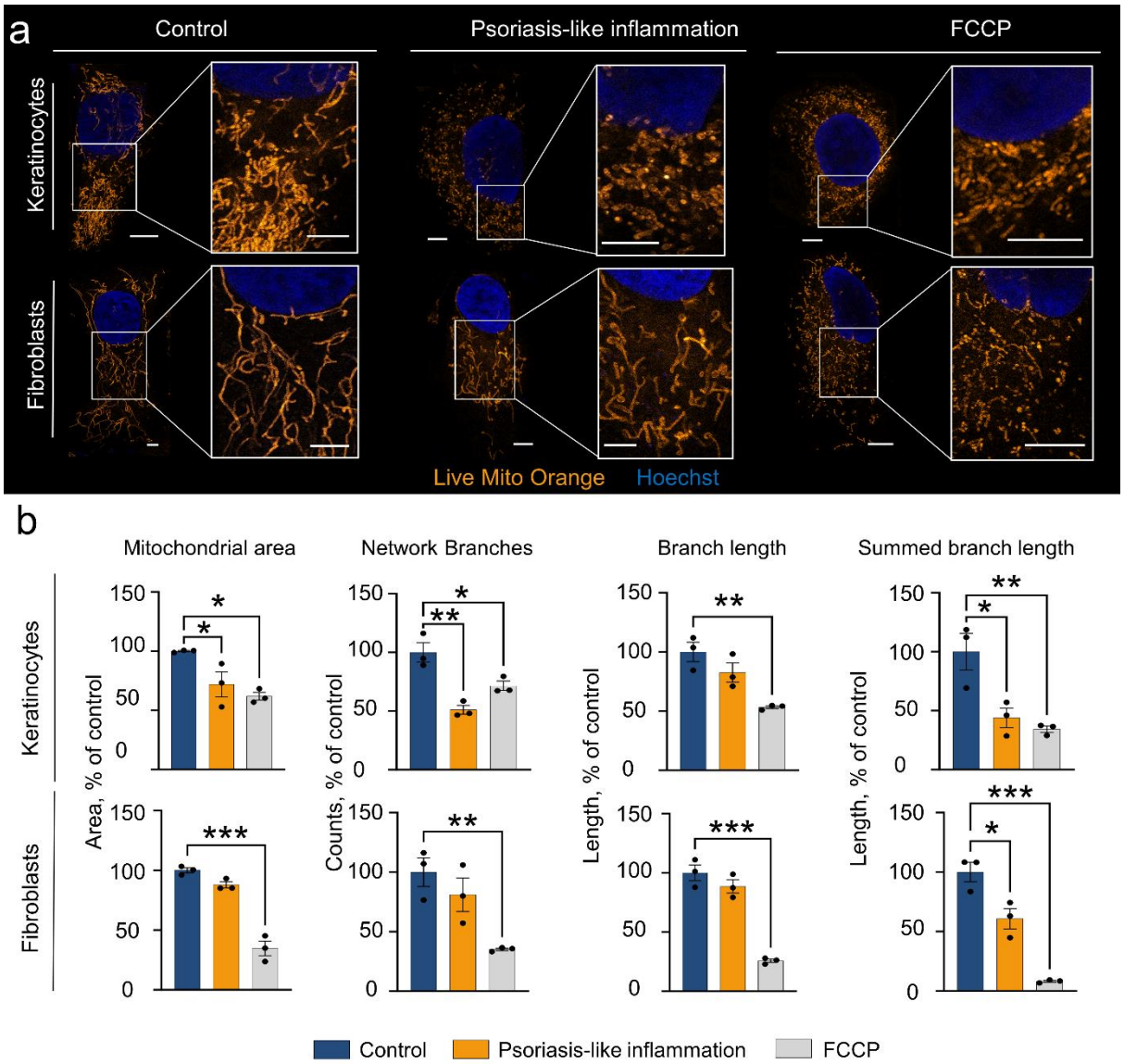

Figure 3. Mitochondrial morphometry of keratinocytes and fibroblasts with psoriasis-like inflammation (PLI).

(a) Represetative STED nanoscopy images of cells labeled with Live Mito Orange. FCCP was used as a positive control.

(b) Mitochondrial network changes were determined by MiNa morphology analysis tool in Fiji. Quantitative results of mitochondrial network parameters. These include mitochondrial area, the mean number of network branches, the mean length of all mitochondrial branches, and the mean of the combined lengths of branches per individual structure. Data represented as mean ± SEM. Statistically significant differences were determined by the one-way ANOVA Dunnett's test. *p< 0.05, ** p <0.01, ***p<0.001, n=3.

Representative images (Figure 3a) show a dramatic fragmentation in PL-KCs, where mitochondria appear vesicle-shaped rather than network-like, while PL-FCs maintained the network shape but showed shorter structures. Quantitative analysis showed a significant decrease in mitochondrial area (28%) and network branches (48%) in PL-KCs compared to control KCs (Figure 3b), while in PL-FCs these parameters remained unchanged. Both cell types displayed decreased summed branch length by 56% and 39% in PL-KCs and PL-FCs, respectively, while overall branch length did not change. This suggests an increased number of individual networks, indicating mitochondrial fragmentation in both PL-cell types.

We compared PLI-induced changes to FCCP-induced fragmentation as a reference for extreme mitochondrial stress (Figure 3b). In KCs, FCCP caused a 38% reduction in mitochondrial area, 28% in network branches, a 46% decrease in branch length and 65% in summed branch length. PLI-induced changes were similar but showed a stronger reduction in network branches (48% vs FCCP's 28%), indicating significant mitochondrial fragmentation in PL-KCs. In FCs, FCCP caused a reduction of 65% in mitochondrial area, 64% in network branches, 74% in branch length, and 91% in summed branch length. These changes were more pronounced than those induced by PLI, indicating relatively moderate mitochondrial fragmentation in PL-FCs.

To determine individual cytokine's role in PLI-induced mitochondrial changes, we exposed cells to either IL-17A, IL-22 or TNF-α (Supplementary figure S3). In KCs, IL-22 caused a 30% reduction in mitochondrial area, similar to the 28% decrease from the cytokine mix, suggesting IL-22 is the primary factor in mitochondrial elimination. However, it did not affect other network parameters. TNF-α caused a 14% reduction in network branches and 18.5% - in summed branch length, indicating this cytokine causes fragmentation, though less so than induced by cytokine mix. In FCs, IL-17A reduced summed branch length by 25%, compared to 39% from the cytokine mix, suggesting IL-17A significantly contributes to

fragmentation in FCs. Notably, the combination of three cytokines caused more pronounced changes than each alone.

The data indicate that PLI-inducing cytokines synergize at mitochondria of both cell types, with KCs exhibiting significantly more pronounced mitochondrial loss and network fragmentation than FCs.

Psoriasis-like inflammation induces mitochondrial swelling and affects cristae architecture

Mitochondrial network changes suggest a possible impact of PLI on mitochondrial cristae organization; thus, we tested if PLI alters cristae morphology and compared changes in PL-KCs and PL-FCs, using Live Mito Orange and STED nanoscopy for super-resolution imaging.

Under PLI, mitochondria appeared swollen with sparsely arranged cristae in both cell types compared to controls (Figure 4b, upper part). Quantitative analysis confirmed a significantly increased mitochondrial width by 10.9% in PL-KCs and 11.4% in PL-FCs (Figure 4c); without changes in cristae area (Figure 4d). Intercristae distance increased by 16.2% in PL-KCs and 12.2% in PL-FCs (Figure 4e). Lastly, the cristae elimination process was confirmed by evaluating the cristae count per 1µm (cristae density), which decreased by 11.5% in PL-KCs and 10.1% in PL-FCs (Figure 4f).

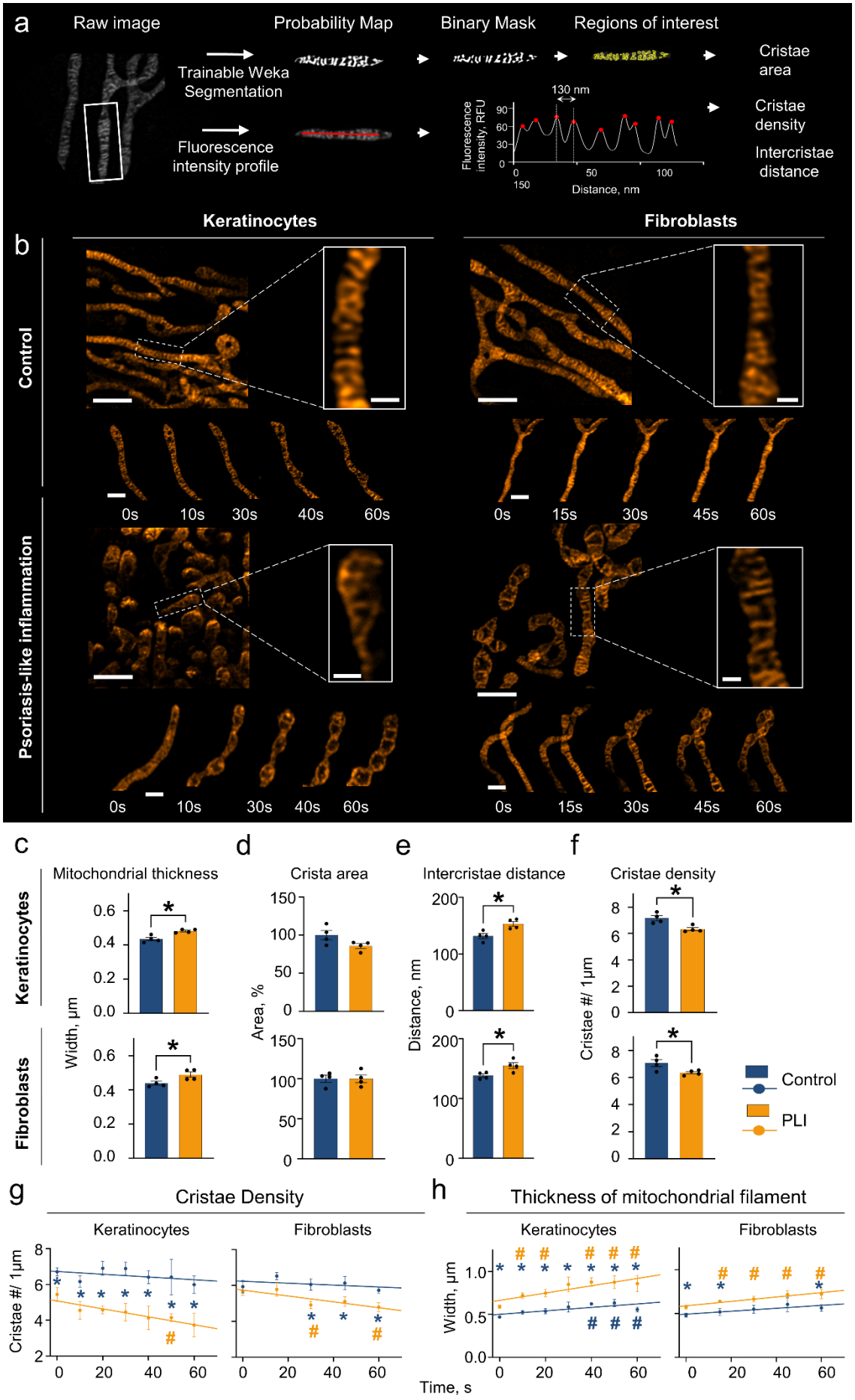
a
Raw image
Probability Map
Binary Mask
Regions of interest
Trainable Weka Segmentation
Fluorescence intensity profile
Cristae area
Cristae density
Intercristae distance
130 nm
Fluorescence intensity, RFU
Distance, nm
b
Keratinocytes
Fibroblasts
Control
Psoriasis-like inflammation
0s
10s
30s
40s
60s
15s
45s
c
Mitochondrial thickness
Width, µm
d
Crista area
Area, %
e
Intercristae distance
Distance, nm
f
Cristae density
Cristae #/ 1µm
Control
PLI
g
Cristae Density
Cristae #/ 1µm
h
Thickness of mitochondrial filament
Width, µm
Time, s

Figure 4. Mitochondrial cristae characteristics of keratinocytes and fibroblasts with psoriasis-like inflammation (PLI).
(a) – Cristae analysis scheme. Cristae area evaluated using Trainable Weka Segmentation, spacing - as average peak (cristae) distances along 1-2µm fluorescence intensity profiles and density as peaks/1µm.
(b) – Overview and time-lapse (Scales: 1µm, 200nm).
(c) – Mitochondrial filament thickness.
(d) – Average crista area. (Control = 100%)
(e) – Intercristae distance.
(f) – Cristae density.
(g) – Cristae density and (h) – mitochondrial thickness change over 60s.
Data: mean ± SEM. Statistics: unpaired, two-tailed Student's t-test. #,*$p < 0.05$, n=4. In (g)**,** (h)**:** blue asterisk (*) indicates a significant difference vs. control at the same time point. A dash (#) - a comparison with the initial time point (0s) within the control (blue #) and the PLI (yellow #) groups.

To determine whether mitochondrial swelling was finite or continuous, we measured changes over 60 seconds. Time-lapse images (Figure 4b, lower part) showed ongoing cristae reduction and mitochondrial filament swelling in PL cells. In PL-KCs, mitochondrial filaments expanded by 20-55% between 10-60s (Figure 4h). Control KCs showed less swelling (18-34%) towards the end of the recording (40-60s). In PL-FCs, mitochondrial filaments expanded by 11-26% between 15-60s, with no further swelling in control FCs. Cristae density in PL cells gradually decreased (Figure 4g): by 23% in PL-KCs at 50s and by 13-15% in PL-FCs between 30-60s. Control KCs and FCs showed no change. Interestingly, cristae density was significantly lower at the moment of observation (0s) in PL-KCs compared to controls, while no initial difference was observed in PL-FCs vs. control. However, cristae density in PL-FCs significantly decreased after 30s, suggesting a delayed process compared to PL-KCs.

Summarizing, PLI caused persistent mitochondrial swelling and a gradual decrease in cristae density in PL cells, with cristae elimination in PL-KCs already in progress and delayed in PL-FCs.

Discussion

In this study, we confirmed that PLI induces cell-type specific mitochondrial dysfunctions. We found that PLI causes (i) a decrease in mitochondrial respiration, as well as glycolysis dysfunction only in PL-KCs, (ii) an increase of mitochondrial ROS production both in PL-KCs and PL-FCs, (iii) a severe degree of mitochondrial fragmentation and mitochondrial area reduction in PL-KCs, while in PL-FCs it causes moderate fragmentation with no changes in mitochondrial area. Lastly (iv), PLI causes mitochondrial filament swelling, resulting in a gradual decline in cristae density in both cell types, with PL-KCs mitochondria being affected more intensively than those of PL-FCs.

PLI treatment significantly upregulated psoriasis-related inflammatory mediators in both cell types, with notable differences in concentration levels. Specifically, PL-KCs had higher SKALP/Elafin and IL-1β concentrations, aligning with their primary expression in psoriatic epidermis [14], [15]. In turn, PL-FCs showed higher concentrations of IL-6 and CXCL8, which is linked to recruiting IL-17A-releasing cells [16]. Despite variations in serum inflammatory mediator levels in psoriasis patients, our results match *in vivo* data ranges [17], [18]. Cell-type specific mitochondrial responses to PLI indicate higher sensitivity of KCs and the delayed reaction of FCs, likely due to their distinct roles. KCs, forming a protective barrier, respond rapidly to stimuli, while FCs, maintaining the extracellular matrix, have slower signaling and metabolic demands [19]. Additionally, psoriatic skin shows increased glycolysis [20], yet PL-KCs exhibited lower glycolytic efficiency. It was reported that miR-31, which is overexpressed in psoriatic epidermis, changes metabolic enzyme expression, resulting in reduced glycolysis [21]. PLI-inducing cytokines can trigger miR-31 expression via NF-κB in HaCaT cells [22], suggesting a similar mechanism in PL-KCs. Understanding these mitochondrial response patterns in KCs and FCs may help identify new targets for psoriasis treatment.

ROS is crucial for psoriatic inflammation development [8]. For example, IL-17A and IL-22 enhanced IL-1β production by activating NLRP3 inflammasome via ROS in HaCaT cells [23]. Psoriasis patients show activated NLRP3 and increased secretion of its downstream cytokines, IL-1β and IL-18 [24]. While we haven't analyzed NLRP3 directly, elevated IL-1β and IL-18 levels in PL-KCs and PL-FCs media suggest this inflammation-related enzyme complex may be involved.

Elevated MitoROS with reduced respiration is linked to excessive mitochondrial fission [25], which we observed in both PL-KCs and PL-FCs. Mitochondrial fission triggers inflammation by regulating pro-inflammatory mediators [26]. For example, in psoriatic macrophages, it activates cytokine production through MAPK and NF-κB pathways, regulated by pro-fission proteins GDAP1L1 and Drp-1 [9]. Our results also showed increased secretion of IFN-γ, cytokines IL-6, IL-1α and chemokines CXCL8 and CCL5 in PL-cells, which might depend on NFκB activation. While no studies have examined mitochondrial morphology in KCs and FCs treated with the cytokine cocktail of this study, TNF-α [27], [28] and IL-17A [29] are known to induce fragmentation via Drp1. Indeed, our analysis revealed TNF-α as the main effector in causing mitochondrial fragmentation in PL-KCs, and IL-17A in PL-FCs. Drp-1 inhibition attenuates TNF-α-induced NF-κB activation [30] and alleviates atopic dermatitis symptoms similar to psoriasis [31]. Our findings suggest a potential link between mitochondrial fission and psoriatic inflammation, which requires further investigation.

Our results, for the first time, showed that psoriasis-like inflammation causes mitochondrial filament swelling, accompanied by cristae elimination in KCs and FCs. In our previous study, we captured similar changes in a viral infection model of human lung microvascular cells [32], suggesting that this may be a general trend of inflammatory response. Transmission electron microscopy (TEM) studies on similar models have shown cristae elimination [28], [33]. However, while TEM can reveal precise intercellular compartment

structures, it cannot capture dynamic processes in living cells. Using STED nanoscopy, we tracked changes in cristae density over time, which allowed us to see a sustained change caused by PLI in both cell types. After 24 hours of PLI-inducing cytokine exposure, PL-KCs showed a clear decrease in cristae density, while PL-FCs exhibited early signs of this process. Cristae restructuring can release mtDNA, activating cGAS/STING and producing type I interferons [34]. Increased production of IFN-α and IFN-β was also found in the media of PL-cells. These interferons, crucial in psoriasis initiation, are overexpressed in patients' blood and lesional skin [35]. Psoriatic patients also show high blood mtDNA levels [36]. These findings suggest a possible link between the disorganization of cristae and psoriatic inflammation, though the activation of the mtDNA/cGAS/STING/IFN pathway in PL-KCs and PL-FCs remains unconfirmed.

The following insights present suggestive directions for future exploration: the observed decrease in mitochondrial respiration in PL-KCs may be linked to reduced cristae density, which can impact respiratory chain complex assembly [37], [38]. However, this connection in PL-KCs remains uncertain. This correlation is unclear in PL-FCs, where cristae density reduction did not affect respiration, possibly due to a delayed response of this process. However, the precise relationship between cristae architecture and mitochondrial function in PL-KC and PL-FC is unknown. Additionally, the decrease in cristae density did not alter their area, suggesting involvement of intramitochondrial fission and fusion process mediated by MICOS complex. These processes might involve dividing or merging individual cristae while maintaining a consistent overall area [39]. Still, the exact mechanism remains unclear. Furthermore, although HaCaT and BJ-5ta cell lines are often used to examine inflammatory responses in the skin [40], [41], it is important to confirm detected changes in patient-derived primary cells in order to test the hypothesis on a larger scale.

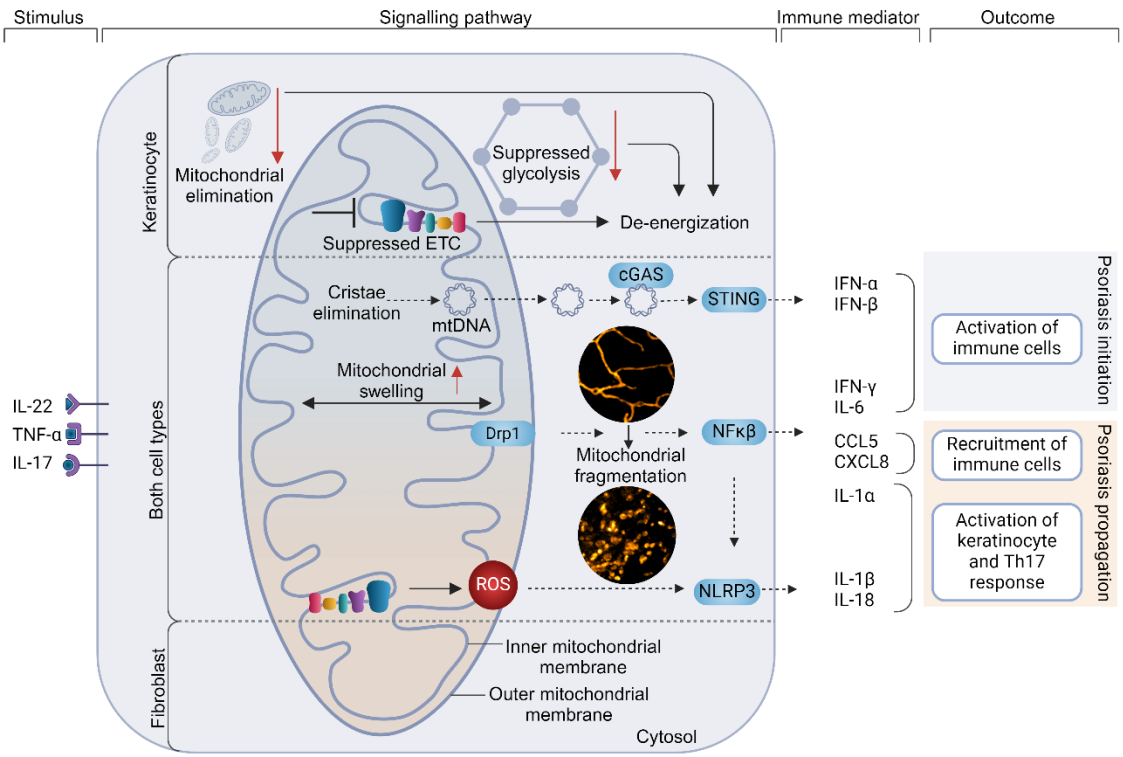

Figure 5. Mitochondrial changes in psoriatic-like keratinocytes and fibroblasts aligned with possible signaling pathways and secreted pro-inflammatory proteins, which contribute to psoriasis pathogenesis. Under psoriasis-like inflammation, both cell types exhibit increased mitochondrial swelling and cristae elimination, potentially resulting in mtDNA release. This activates the cGAS/STING and type I interferon production, which stimulates immune cells, leading to psoriasis initiation. Mitochondrial fragmentation, often Drp-1 dependent, may activate NF-κB, resulting in cytokine production that drives disease propagation by recruiting immune cells and activating keratinocyte and Th17 cell response. MitoROS activation can also contribute to this process by activating NLRP3 inflammasome and IL-1β and IL-18 secretion. Psoriatic-like keratinocytes exhibit mitochondrial elimination, suppressed electron transport chain (ETC) activity, and glycolysis, indicating cell-type-specific de-energization.

In conclusion, our study reveals that psoriasis-like inflammation in keratinocytes and fibroblasts induces mitochondrial changes, such as increased MitoROS production, mitochondrial fragmentation, swelling, and cristae remodeling, which can contribute to psoriasis by regulating the production of pro-inflammatory mediators (Figure 5). Importantly, keratinocytes exhibit a more sensitive mitochondrial response to psoriatic-like inflammation compared to psoriatic-like fibroblasts. Further investigations are required to confirm the mechanistic link between mitochondrial changes and inflammatory responses in these cells.

Also, it is important to determine the role of mitochondrial cristae in modulating mitochondrial functions to provide possible targets for managing psoriasis.

Materials and Methods

The names and catalogue numbers of all reagent manufacturers are provided in Table 1.

REAGENT or RESOURCE	SOURCE	IDENTIFIER
Chemicals, peptides, and recombinant proteins		
TNF-α	Sigma-Aldrich	SRP3177
IL-22	Sigma-Aldrich	SRP3177
IL-17	Sigma-Aldrich	SRP3080
DMEM, high glucose, GlutaMAX supplement	Gibco	10566016
Fetal bovine serum (FBS)	Gibco	26140079
Penicillin/streptomycin	Sigma	P0781
Trypin-EDTA	Gibco	25300054
Hank's Balanced Salt Solution (HBSS)	Gibco	14025092
Hoechst 33342	Invitrogen	H21492
Mito Live Orange	Abberior, Göttingen, Germany	LVORANGE -0146- 30NMOL
MitoSOX	Invitrogen	M36008
Seahorse XF DMEM	Agilent Technologies	103680-100
Bradford Reagent	Sigma	B6916
MitoTempo	Sigma	SML0737
FCCP	Sigma	C2920
Critical commercial assays		
XFp Cell Mito Stress test kit	Agilent Technologies	103025-100
PureLink RNA mini kit	Invitrogen, Thermo Fisher Scientific, Bleiswijk, The Netherlands	12183020
DNAse I	Thermo Fisher Scientific, Vilnius, Lithuania	EN0521
High-Capacity Reverse Transcription kit	Life Technologies, Thermo Fisher Scientific, Bleiswijk, The Netherlands	4368814
Power SYBR Green PCR mix	Thermo Fisher Scientific, Vilnius, Lithuanian	4368577
Human Custom ProcartaPlex kit	Thermo Fisher Scientific, Waltham, MA.	PPX-15-MXWCXW6
Presto Blue Viability Reagent	Invitrogen, Life Technologies Limited, Cambridge, UK	A13261
Experimental models: Cell lines		
HaCaT Keratinocytes	CLS Cell Lines Service GmbH, Eppelheim, Germany	300493
BJ-5ta Fibroblasts	ATCC, Manassas, VA, USA	CRL-4001
Oligonucleotides		

PI3 target, forward primer: CTTCTTGATCGTGGTGGTGTTC	Thermo Fisher Scientific	N/A
PI3 target, reverse primer: AACGGGATCTTGTCCATTGAAT	Thermo Fisher Scientific	N/A
GAPDH target, forward primer: TCAAGATCATCAGCAATGCCT	Thermo Fisher Scientific	N/A
GAPDH target, reverse primer: CATGAGTCCCACGATACC	Thermo Fisher Scientific	N/A
Software and algorithms		
Fiji Image Analysis	ImageJ	https://imagej.net/Fiji
Graph pad prism version 10	Graph Pad	https://www.graphpad.com
Huygens Software	Scientific Volume Imaging B.V	https://svi.nl/Huygens-Software
Other		
Petri dishes P35	VWR	75856-742
Seahorse XFp Cell Culture Miniplates	Agilent Technologies	103025-100
Seahorse XFp FluxPak	Agilent Technologies	103022-100

Table 1. Key resources

Cell cultures and treatments

Human skin cells keratinocytes (HaCaT) and fibroblasts (BJ-5ta) were maintained in complete culture media containing DMEM with 10% fetal bovine serum and 1% penicillin/streptomycin at 37 °C. For PLI induction, the next day after plating, cell media was supplemented with cytokines for 24h: TNF-α (5 ng/ml), IL-22 (10 ng/ml), IL-17 (10 ng/ml), from Sigma-Aldrich. PBS was used as a vehicle control.

Gene expression

Total RNA was isolated using the PureLink RNA mini kit followed by DNAse I treatment to remove DNA traces. Reverse transcription was performed using the High-Capacity Reverse Transcription kit. Real-time PCR was conducted with Power SYBR Green PCR mix on a Rotor-Gene-Q System (Qiagen) using the $2^{(-\Delta\Delta Ct)}$ method for relative gene

expression analysis, with glyceraldehyde 3-phosphate dehydrogenase (GAPDH) as the endogenous control. Results depicted in Log2 Fold Change form.

Protein secretion

For protein secretion analysis Human Custom ProcartaPlex kit was used with Luminex 200 instrument (Luminex Corp, Austin, TX) following the manufacturer's instructions. xPONENT software facilitated assessment. Mean fluorescence intensities (MFIs) were converted to concentrations (pg/ml) using the standard range equation for the relevant analyte. Values exceeding the detection limit were substituted with the highest standard concentration.

Cellular respiration

Cells were seeded at 5000 cells per well in Seahorse XFp cell culture plates and treated with PLI-inducing cytokines for 24h. Bioenergetic function was evaluated using the Seahorse XFp Analyzer (Agilent Technologies, Santa Clara, CA, USA) with the Seahorse XFp Cell Mito Stress Test Kit. The assay was conducted according to the manufacturer's instructions. More detailed information is available on the website (https://www.agilent.com/en/product/cell-analysis/real-time-cell-metabolic-analysis/xf-assay-kits-reagents-cell-assay-media/seahorse-xf-cell-mito-stress-test-kit-740885). Final concentrations of electron transport chain-targeting compounds: 1.5 µM oligomycin, 0.5 µM FCCP, and 0.5 µM rotenone and antimycin A. Results were normalized to total cellular protein content determined with the Bradford reagent (Sigma) and assessed using a multifunctional plate reader Infinite 200 Pro Nano Plex (Tecan, Männedorf, Switzerland).

Cell metabolic activity

Cells were seeded at 5000 cells per well in 96-well plates and treated as previously described. Metabolic activity was assessed using PrestoBlue™ Cell Viability Reagent following the manufacturer's instructions. After 24, 48, and 72 hours of incubation, cell media

was replaced with a solution containing 10% PrestoBlue reagent and 90% cell culture media. After a 40-minute incubation at 37 °C in the dark, fluorescence was measured using a plate reader (Infinite 200 Pro M Nano Plex, Tecan, Männedorf, Switzerland) at excitation and emission wavelengths of 560 nm and 590 nm, respectively. The metabolic activity of the control group was considered as 100%.

Mitochondrial superoxide determination

Cells were stained with 2 µM MitoSox Red in HBSS at 37 °C for 30min, followed by two washes. Fluorescent images were captured using an Olympus APX100 microscope, and Fiji was used for fluorescence intensity assessment. MitoTempo (Sigma), a mitochondrial ROS scavenger, was used at 20 µM, added 1h before cytokine treatment, and co-incubated for 24h. Antimycin A (Sigma), a superoxide inducer, was used at 50 µM for 10min as a positive control. In Fiji, fluorescence intensity was measured using threshold-based segmentation (Huang algorithm). MitoSOX fluorescence in the control group was set at 100%.

Mitochondrial morphometry

Cells cultured in glass-bottom Petri dishes at a density of 4 x 10^4. To visualize mitochondrial structures, cells were stained with 100 nM Mito Live Orange for 40min in a medium without FBS, followed by washing and imaging in HBSS using using Zeiss Axio Observer.Z1 (Zeiss, Oberkochen, Germany) and Olympus IX83 (Olympus Corporation, Tokyo, Japan) fluorescent microscopes. FCCP at 0.2 µM for 10min induced extensive fragmentation. Mitochondrial morphology parameters (Supplemental Figure S2) were quantitatively assessed using the Fiji plugin Mitochondrial Network Analysis (MiNa) toolset [42], including mitochondrial area, mean of network branches, mean branch length, and mean of summed branch lengths. At least 10 cells per experimental group in three repeats were analyzed.

Cristae imaging and analysis

Cells were plated and stained with Mito Live Orange, as indicated previously. Imaging was performed using a STEDYCON system (Abberior Instruments GmbH, Göttingen, Germany) equipped with an Olympus IX83 microscope, a 100x oil immersion objective with a NA 1.45. Cristae area, density and spacing were assessed following steps depicted in Figure 4a). For cristae imaging, image acquisition employed 10-30 pixel sizes. Image size varied from 5 µm x 5 µm to 10 µm x 10 µm. Fluorescence signal accumulation employed 2-5 line steps with dwell times of 10 µs, and a pinhole set at 40 µm. For time-lapse recording, images were captured with a frame interval of 10-15 s for 60s. Compensation for photobleaching was carried out by bleach correction feature in Fiji. Subsequently, acquired images were subjected to deconvolution using Huygens software (Scientific Volume Imaging B.V., Hilversum, The Netherlands).

For average crista area measurement, cristae were segmented using the Trainable Weka Segmentation Tool in Fiji, following the guidelines provided in a paper [43]. Briefly, the plugin generated a probability map highlighting potential cristae areas compared to the background. These areas were then thresholded to create binary masks and processed using the "Watershed" function. Afterward, the "Analyze Particles" function outlined and marked cristae structures as regions of interest (ROIs). Finally, these structures were overlaid onto the original image and measured. Cristae spacing and density were assessed by analyzing fluorescence intensity profiles along 1-2 µm line segments. For mitochondrial thickness assessment, intensity profiles were plotted across the mitochondrial width. At least three line profiles were measured for cristae analysis, while another three -were used to evaluate the width of the mitochondrial filament in each image. ROIs for plotting fluorescence intensity profiles depended on cristae clarity, where mitochondrial filaments were not entangled, coiled, or of the focal point. Intercristae distance was determined by the distance between fluorescence

peaks, and cristae density was calculated as the number of peaks per 1 µm segment. Fluorescence peaks were identified using Fiji's BAR macro "Find peaks". Time-dependent analysis involved fluorescence intensity profile measurement in each frame of the time-lapse. At least 10 cells per experimental group in four experimental repeats were examined, and analysis was conducted on randomly chosen regions. For time-lapse analysis, 4-6 video recordings were analyzed.

Quantification and statistical analysis

Statistical analysis comprised at least three independent biological experiments with a minimum of two technical replicates each. Pairwise comparisons used an unpaired, two-tailed Student's t-test. For three-group comparisons, we applied one-way ANOVA with Tukey's test for inter-group comparisons and Dunnett's test for comparisons with the control. Grouped data underwent analysis using two-way ANOVA, followed by an uncorrected Fisher's LSD test. The data analysis utilized GraphPad Prism software, version 10.0 (GraphPad Software, Inc., USA).

Data Availability Statement

No datasets were generated or analyzed during the current study. Any additional information required to reanalyze the data reported in this work paper is available from the lead contact upon request.

Acknowledgements

This work was supported by the Research Fund of the Lithuanian University of Health Sciences. This project has received funding from the Research Council of Lithuania (LMTLT), agreement No: S-A-UEI-23-7. Illustrations were created using BioRender.com.

Author Contributions Statement

Conceptualization, A.J., and R.M; Methodology, G.K.; Formal analysis, G.K., M.U., S.H., M.K., J.Š., and V.Š.; Investigation, G.K., M.U., S.H., M.K., J.Š. and V.Š.; Resources, A.J., R.M.; Writing - original draft preparation, G.K. and A.J.; Writing - review and editing, G.K., A.J. and R.M.; Visualization, G.K., and A.J.; Supervision, A.J., R.M.; Project Administration: A.J.; Funding acquisition: A.J. All authors have read and agreed to the published version of the manuscript.

References

[1] F. Ma *et al.*, 'Single cell and spatial sequencing define processes by which keratinocytes and fibroblasts amplify inflammatory responses in psoriasis', *Nat. Commun.*, vol. 14, no. 1, Art. no. 1, Jun. 2023, doi: 10.1038/s41467-023-39020-4.

[2] F.-X. Bernard *et al.*, 'Keratinocytes under Fire of Proinflammatory Cytokines: Bona Fide Innate Immune Cells Involved in the Physiopathology of Chronic Atopic Dermatitis and Psoriasis', *J. Allergy*, vol. 2012, p. e718725, Nov. 2012, doi: 10.1155/2012/718725.

[3] X. Zhou, Y. Chen, L. Cui, Y. Shi, and C. Guo, 'Advances in the pathogenesis of psoriasis: from keratinocyte perspective', *Cell Death Dis.*, vol. 13, no. 1, Art. no. 1, Jan. 2022, doi: 10.1038/s41419-022-04523-3.

[4] M. Alecu, G. Coman, A. Mușetescu, and O. A. Coman, 'Antimicrobial peptides as an argument for the involvement of innate immunity in psoriasis (Review)', *Exp. Ther. Med.*, vol. 20, no. 6, pp. 1–1, Dec. 2020, doi: 10.3892/etm.2020.9322.

[5] J. A. C. Alkemade *et al.*, 'SKALP/elafin is an inducible proteinase inhibitor in human epidermal keratinocytes', *J. Cell Sci.*, vol. 107, no. 8, pp. 2335–2342, Aug. 1994, doi: 10.1242/jcs.107.8.2335.

[6] H. A. Alkemade, G. J. de Jongh, W. P. Arnold, P. C. van de Kerkhof, and J. Schalkwijk, 'Levels of skin-derived antileukoproteinase (SKALP)/elafin in serum correlate with disease activity during treatment of severe psoriasis with cyclosporin A', *J. Invest. Dermatol.*, vol. 104, no. 2, pp. 189–193, Feb. 1995, doi: 10.1111/1523-1747.ep12612749.

[7] M. C. Ovejero-Benito *et al.*, 'Polymorphisms associated with optimization of biological therapy through drug dose reduction in moderate-to-severe psoriasis', *J. Eur. Acad. Dermatol. Venereol. JEADV*, vol. 34, no. 6, pp. e271–e275, Jun. 2020, doi: 10.1111/jdv.16256.

[8] S. Mizuguchi *et al.*, 'Mitochondrial Reactive Oxygen Species Are Essential for the Development of Psoriatic Inflammation', *Front. Immunol.*, vol. 12, p. 714897, Aug. 2021, doi: 10.3389/fimmu.2021.714897.

[9] A. Alalaiwe, C.-Y. Chen, Z.-Y. Chang, J.-T. Sung, S.-Y. Chuang, and J.-Y. Fang, 'Psoriasiform Inflammation Is Associated with Mitochondrial Fission/GDAP1L1 Signaling in Macrophages', *Int. J. Mol. Sci.*, vol. 22, no. 19, p. 10410, Sep. 2021, doi: 10.3390/ijms221910410.

[10] N. Baker, J. Patel, and M. Khacho, 'Linking mitochondrial dynamics, cristae remodeling and supercomplex formation: How mitochondrial structure can regulate

bioenergetics', *Mitochondrion*, vol. 49, pp. 259–268, Nov. 2019, doi: 10.1016/j.mito.2019.06.003.
[11] M. Chen *et al.*, 'Mitophagy receptor FUNDC1 regulates mitochondrial dynamics and mitophagy', *Autophagy*, vol. 12, no. 4, pp. 689–702, Apr. 2016, doi: 10.1080/15548627.2016.1151580.
[12] D. S. Umbaugh, N. T. Nguyen, H. Jaeschke, and A. Ramachandran, 'Mitochondrial Membrane Potential Drives Early Change in Mitochondrial Morphology After Acetaminophen Exposure', *Toxicol. Sci.*, vol. 180, no. 1, pp. 186–195, Jan. 2021, doi: 10.1093/toxsci/kfaa188.
[13] X. Liu and G. Hajnóczky, 'Altered fusion dynamics underlie unique morphological changes in mitochondria during hypoxia–reoxygenation stress', *Cell Death Differ.*, vol. 18, no. 10, Art. no. 10, Oct. 2011, doi: 10.1038/cdd.2011.13.
[14] K. Nonomura, K. Yamanishi, H. Yasuno, K. Nara, and S. Hirose, 'Up-regulation of elafin/SKALP gene expression in psoriatic epidermis', *J. Invest. Dermatol.*, vol. 103, no. 1, pp. 88–91, Jul. 1994, doi: 10.1111/1523-1747.ep12391802.
[15] Y. Cai *et al.*, 'A Critical Role of the IL-1β-IL-1R Signaling Pathway in Skin Inflammation and Psoriasis Pathogenesis', *J. Invest. Dermatol.*, vol. 139, no. 1, pp. 146–156, Jan. 2019, doi: 10.1016/j.jid.2018.07.025.
[16] C. Angiolilli *et al.*, 'ZFP36 Family Members Regulate the Proinflammatory Features of Psoriatic Dermal Fibroblasts', *J. Invest. Dermatol.*, vol. 142, no. 2, pp. 402–413, Feb. 2022, doi: 10.1016/j.jid.2021.06.030.
[17] M. Forouzandeh, J. Besen, R. W. Keane, and J. P. de Rivero Vaccari, 'The Inflammasome Signaling Proteins ASC and IL-18 as Biomarkers of Psoriasis', *Front. Pharmacol.*, vol. 11, Aug. 2020, doi: 10.3389/fphar.2020.01238.
[18] N. O. Kurtovic and E. K. Halilovic, 'Serum Concentrations of Interferon Gamma (IFN-γ) in Patients with Psoriasis: Correlation with Clinical Type and Severity of the Disease', *Med. Arch.*, vol. 72, no. 6, pp. 410–413, Dec. 2018, doi: 10.5455/medarh.2018.72.410-413.
[19] A. V. Nguyen and A. M. Soulika, 'The Dynamics of the Skin's Immune System', *Int. J. Mol. Sci.*, vol. 20, no. 8, p. 1811, Apr. 2019, doi: 10.3390/ijms20081811.
[20] Y. Liu *et al.*, 'Pyruvate Kinase M2 Mediates Glycolysis Contributes to Psoriasis by Promoting Keratinocyte Proliferation', *Front. Pharmacol.*, vol. 12, p. 765790, Oct. 2021, doi: 10.3389/fphar.2021.765790.
[21] M. Wang *et al.*, 'Metabolic rewiring in keratinocytes by miR-31-5p identifies therapeutic intervention for psoriasis', *EMBO Mol. Med.*, vol. 15, no. 4, p. e15674, Apr. 2023, doi: 10.15252/emmm.202215674.
[22] S. Yan *et al.*, 'NF-κB-induced microRNA-31 promotes epidermal hyperplasia by repressing protein phosphatase 6 in psoriasis', *Nat. Commun.*, vol. 6, p. 7652, Jul. 2015, doi: 10.1038/ncomms8652.
[23] K.-A. Cho, J. W. Suh, K. H. Lee, J. L. Kang, and S.-Y. Woo, 'IL-17 and IL-22 enhance skin inflammation by stimulating the secretion of IL-1β by keratinocytes via the ROS-NLRP3-caspase-1 pathway', *Int. Immunol.*, vol. 24, no. 3, pp. 147–158, Mar. 2012, doi: 10.1093/intimm/dxr110.
[24] A. Shahi, S. Afzali, A. Amirzargar, P. Mohaghegh, S. Salehi, and Y. Mansoori, 'Potential roles of inflammasomes in the pathophysiology of Psoriasis: A comprehensive review', *Mol. Immunol.*, vol. 161, pp. 44–60, Sep. 2023, doi: 10.1016/j.molimm.2023.06.007.
[25] D. Li *et al.*, 'Novel Insights and Current Evidence for Mechanisms of Atherosclerosis: Mitochondrial Dynamics as a Potential Therapeutic Target', *Front. Cell Dev. Biol.*, vol. 9, p. 673839, Jul. 2021, doi: 10.3389/fcell.2021.673839.

[26] J. Park *et al.*, ‘Mitochondrial dynamics modulate the expression of pro-inflammatory mediators in microglial cells’, *J. Neurochem.*, vol. 127, Jul. 2013, doi: 10.1111/jnc.12361.
[27] Y.-L. Shen *et al.*, ‘TNF-α induces Drp1-mediated mitochondrial fragmentation during inflammatory cardiomyocyte injury’, *Int. J. Mol. Med.*, vol. 41, no. 4, pp. 2317–2327, Apr. 2018, doi: 10.3892/ijmm.2018.3385.
[28] X.-H. Chen *et al.*, ‘TNF-α induces mitochondrial dysfunction in 3T3-L1 adipocytes’, *Mol. Cell. Endocrinol.*, vol. 328, no. 1, pp. 63–69, Oct. 2010, doi: 10.1016/j.mce.2010.07.005.
[29] J. Zhou *et al.*, ‘IL-17 induces cellular stress microenvironment of melanocytes to promote autophagic cell apoptosis in vitiligo’, *FASEB J.*, vol. 32, no. 9, pp. 4899–4916, 2018, doi: 10.1096/fj.201701242RR.
[30] S. J. Forrester *et al.*, ‘Mitochondrial Fission Mediates Endothelial Inflammation’, *Hypertens. Dallas Tex 1979*, vol. 76, no. 1, pp. 267–276, Jul. 2020, doi: 10.1161/HYPERTENSIONAHA.120.14686.
[31] L. Li, Z. Mu, P. Liu, Y. Wang, F. Yang, and X. Han, ‘Mdivi-1 alleviates atopic dermatitis through the inhibition of NLRP3 inflammasome’, *Exp. Dermatol.*, vol. 30, no. 12, pp. 1734–1744, 2021, doi: 10.1111/exd.14412.
[32] G. Kulkovienė *et al.*, ‘Differential Mitochondrial, Oxidative Stress and Inflammatory Responses to SARS-CoV-2 Spike Protein Receptor Binding Domain in Human Lung Microvascular, Coronary Artery Endothelial and Bronchial Epithelial Cells’, *Int. J. Mol. Sci.*, vol. 25, no. 6, Art. no. 6, Jan. 2024, doi: 10.3390/ijms25063188.
[33] W.-Q. Feng *et al.*, ‘IL-17A-mediated mitochondrial dysfunction induces pyroptosis in colorectal cancer cells and promotes CD8 + T-cell tumour infiltration’, *J. Transl. Med.*, vol. 21, no. 1, p. 335, May 2023, doi: 10.1186/s12967-023-04187-3.
[34] B. He *et al.*, ‘Mitochondrial cristae architecture protects against mtDNA release and inflammation’, *Cell Rep.*, vol. 41, no. 10, Dec. 2022, doi: 10.1016/j.celrep.2022.111774.
[35] H. Gu, Y. Zhang, W. Zeng, and Y. Xia, ‘Participation of interferons in psoriatic inflammation’, *Cytokine Growth Factor Rev.*, vol. 64, pp. 12–20, Apr. 2022, doi: 10.1016/j.cytogfr.2021.12.002.
[36] A. Therianou *et al.*, ‘Mitochondrial dysfunction in affected skin and increased mitochondrial DNA in serum from patients with psoriasis’, *Exp. Dermatol.*, vol. 28, no. 1, pp. 72–75, 2019, doi: 10.1111/exd.13831.
[37] S. Cogliati *et al.*, ‘Mitochondrial cristae shape determines respiratory chain supercomplexes assembly and respiratory efficiency’, *Cell*, vol. 155, no. 1, pp. 160–171, Sep. 2013, doi: 10.1016/j.cell.2013.08.032.
[38] R. Quintana-Cabrera, I. Manjarrés-Raza, C. Vicente-Gutiérrez, M. Corrado, J. P. Bolaños, and L. Scorrano, ‘Opa1 relies on cristae preservation and ATP synthase to curtail reactive oxygen species accumulation in mitochondria’, *Redox Biol.*, vol. 41, p. 101944, Mar. 2021, doi: 10.1016/j.redox.2021.101944.
[39] A. K. Kondadi *et al.*, ‘Cristae undergo continuous cycles of membrane remodelling in a MICOS-dependent manner’, *EMBO Rep.*, vol. 21, no. 3, p. e49776, Mar. 2020, doi: 10.15252/embr.201949776.
[40] H. Zheng *et al.*, ‘Establishing Transcription Profile of Psoriasiform Cutaneous In Vitro using HaCaT Cells Stimulated with Combination of Cytokines’, *J. Vis. Exp. JoVE*, no. 169, Mar. 2021, doi: 10.3791/61537.
[41] L. Pereira da Silva, B. Miguel Neves, L. Moura, M. T. Cruz, and E. Carvalho, ‘Neurotensin Decreases the Proinflammatory Status of Human Skin Fibroblasts and Increases Epidermal Growth Factor Expression’, *Int. J. Inflamm.*, vol. 2014, no. 1, p. 248240, 2014, doi: 10.1155/2014/248240.

[42] A. J. Valente, L. A. Maddalena, E. L. Robb, F. Moradi, and J. A. Stuart, ‘A simple ImageJ macro tool for analyzing mitochondrial network morphology in mammalian cell culture’, *Acta Histochem.*, vol. 119, no. 3, pp. 315–326, Apr. 2017, doi: 10.1016/j.acthis.2017.03.001.
[43] M. Segawa *et al.*, ‘Quantification of cristae architecture reveals time-dependent characteristics of individual mitochondria’, *Life Sci. Alliance*, vol. 3, no. 7, p. e201900620, Jun. 2020, doi: 10.26508/lsa.201900620.

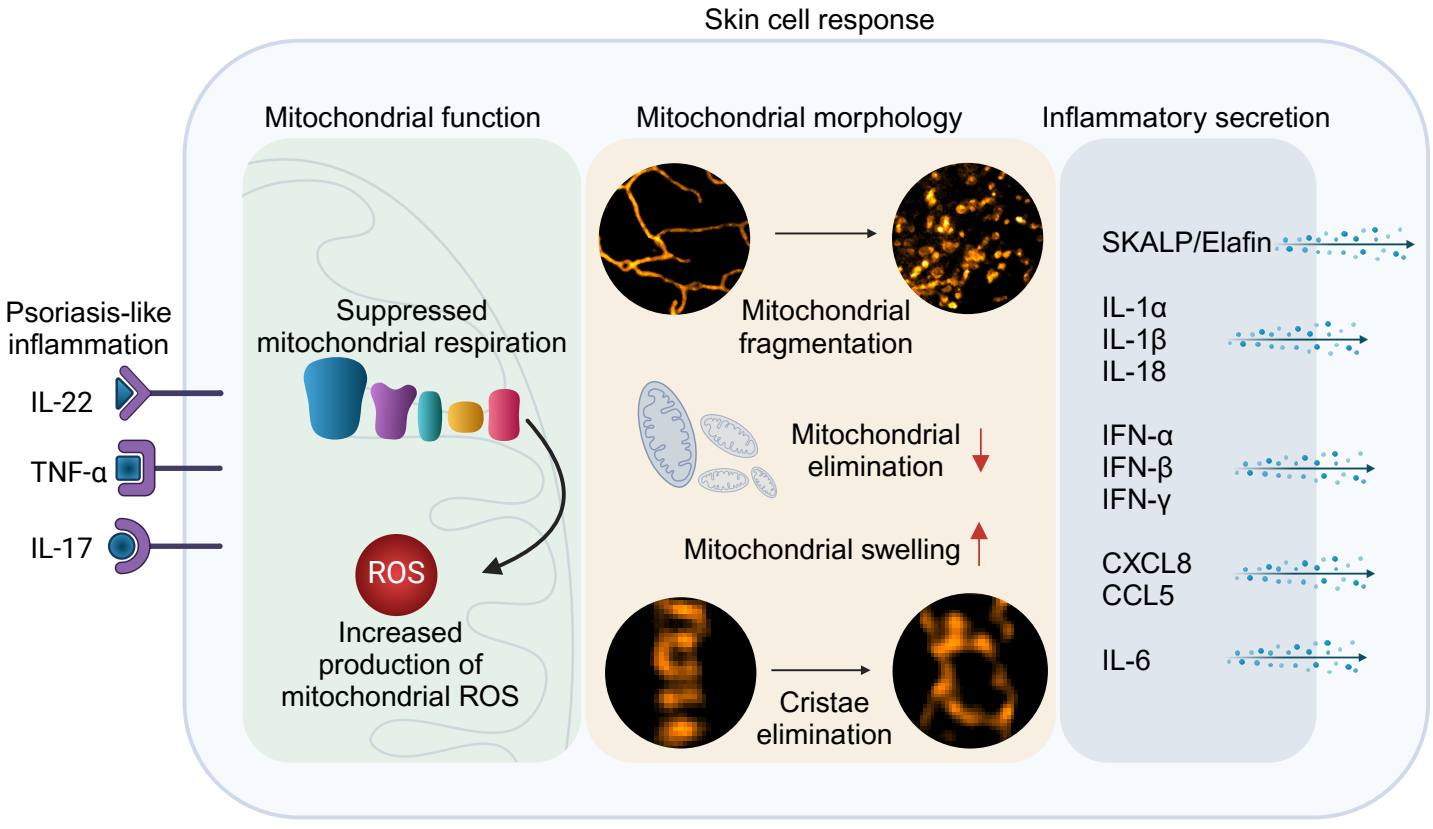
Skin cell response
Mitochondrial function
Mitochondrial morphology
Inflammatory secretion
Psoriasis-like inflammation
IL-22
TNF-α
IL-17
Suppressed mitochondrial respiration
ROS
Increased production of mitochondrial ROS
Mitochondrial fragmentation
Mitochondrial elimination
Mitochondrial swelling
Cristae elimination
SKALP/Elafin
IL-1α
IL-1β
IL-18
IFN-α
IFN-β
IFN-γ
CXCL8
CCL5
IL-6

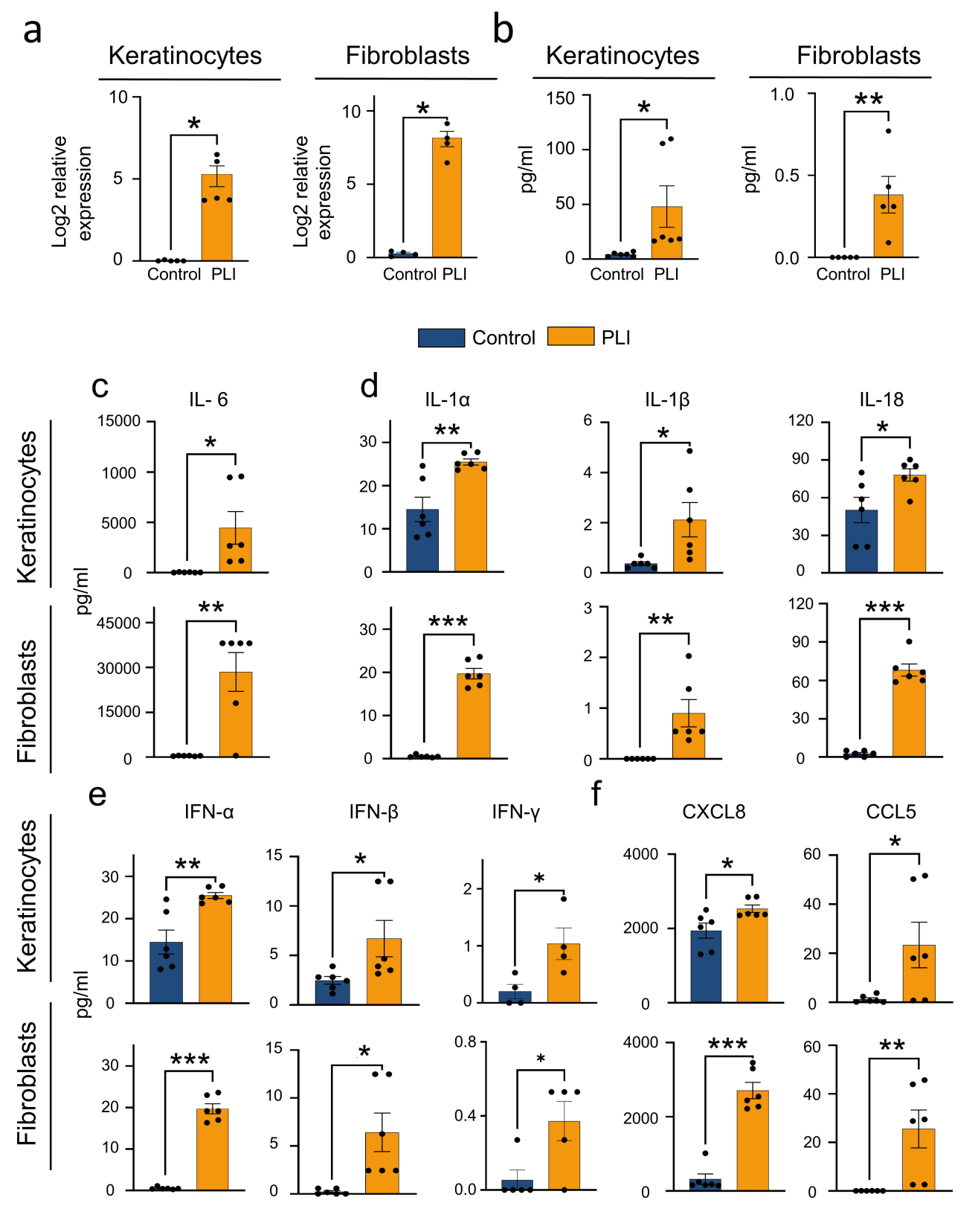
a
Keratinocytes
Fibroblasts
Log2 relative expression
Control
PLI
b
pg/ml
c
IL- 6
d
IL-1α
IL-1β
IL-18
Keratinocytes
Fibroblasts
e
IFN-α
IFN-β
IFN-γ
f
CXCL8
CCL5
Control
PLI

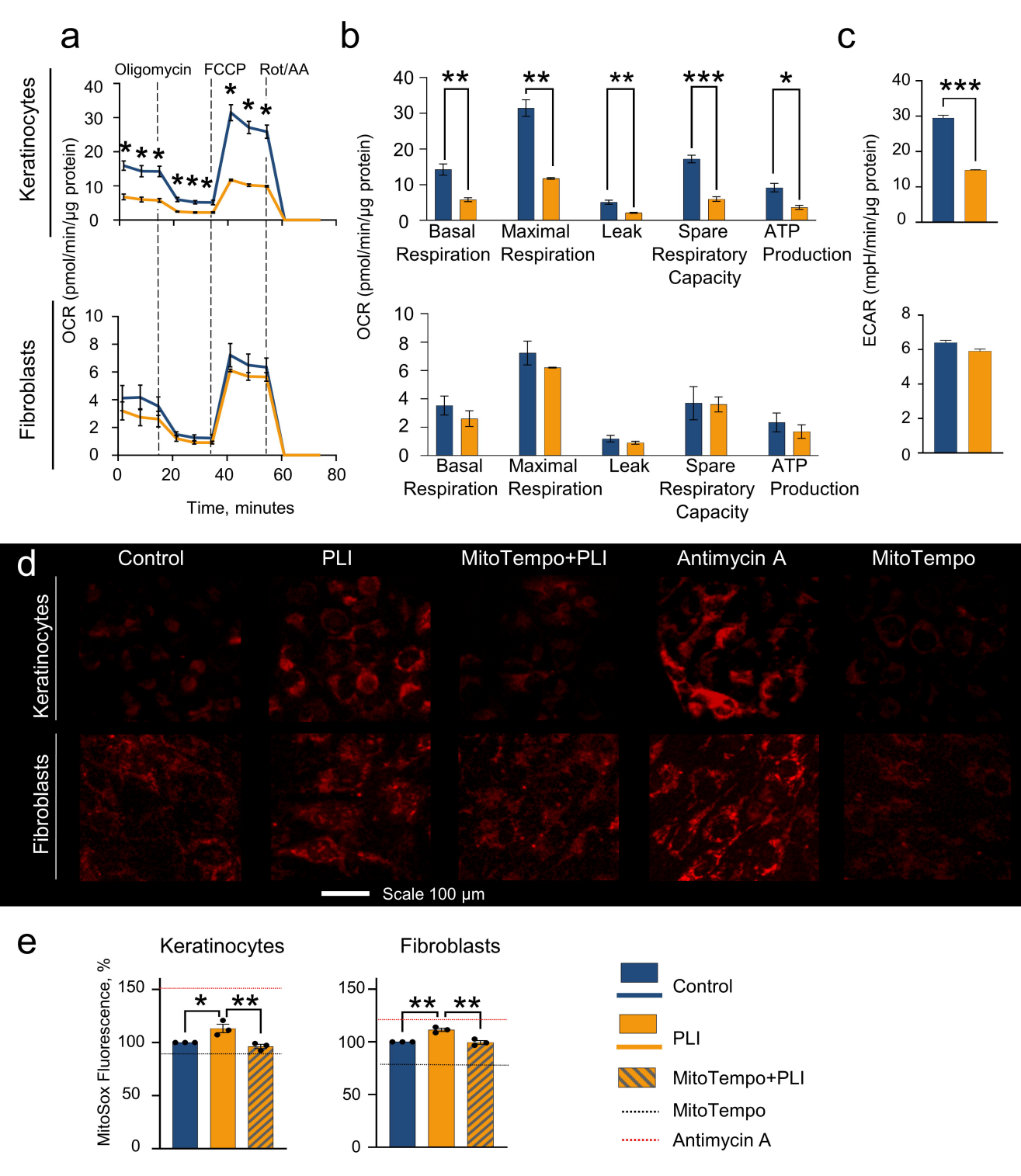
a
Oligomycin
FCCP
Rot/AA
Keratinocytes
Fibroblasts
OCR (pmol/min/µg protein)
Time, minutes
b
Basal Respiration
Maximal Respiration
Leak
Spare Respiratory Capacity
ATP Production
OCR (pmol/min/µg protein)
c
ECAR (mpH/min/µg protein)
d
Control
PLI
MitoTempo+PLI
Antimycin A
MitoTempo
Keratinocytes
Fibroblasts
Scale 100 µm
e
Keratinocytes
Fibroblasts
MitoSox Fluorescence, %
Control
PLI
MitoTempo+PLI
MitoTempo
Antimycin A

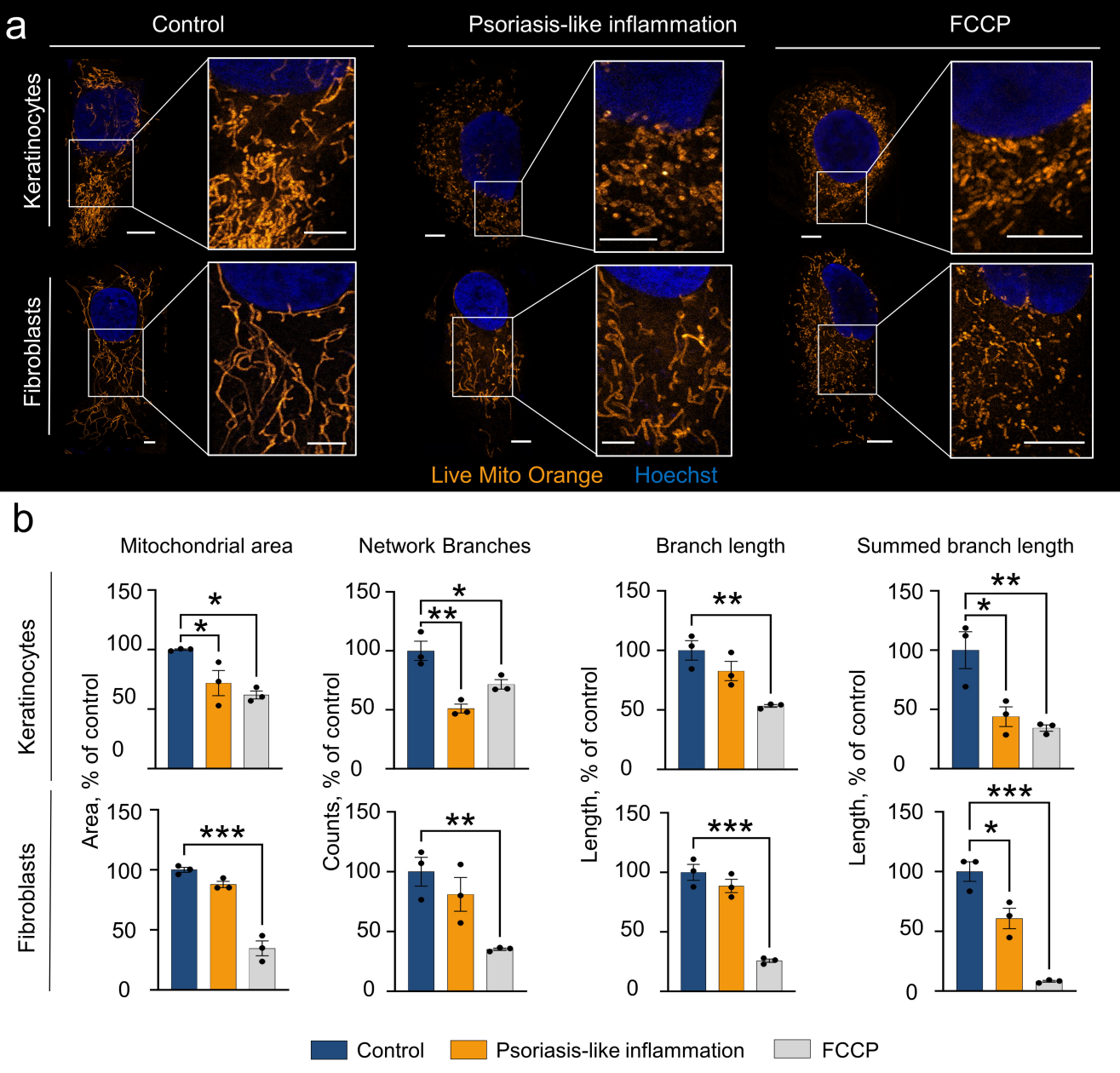
a
Control
Psoriasis-like inflammation
FCCP
Keratinocytes
Fibroblasts
Live Mito Orange
Hoechst
b
Mitochondrial area
Network Branches
Branch length
Summed branch length
Keratinocytes
Fibroblasts
Area, % of control
Counts, % of control
Length, % of control
Length, % of control
150
100
50
0
*
**
***
Control
Psoriasis-like inflammation
FCCP

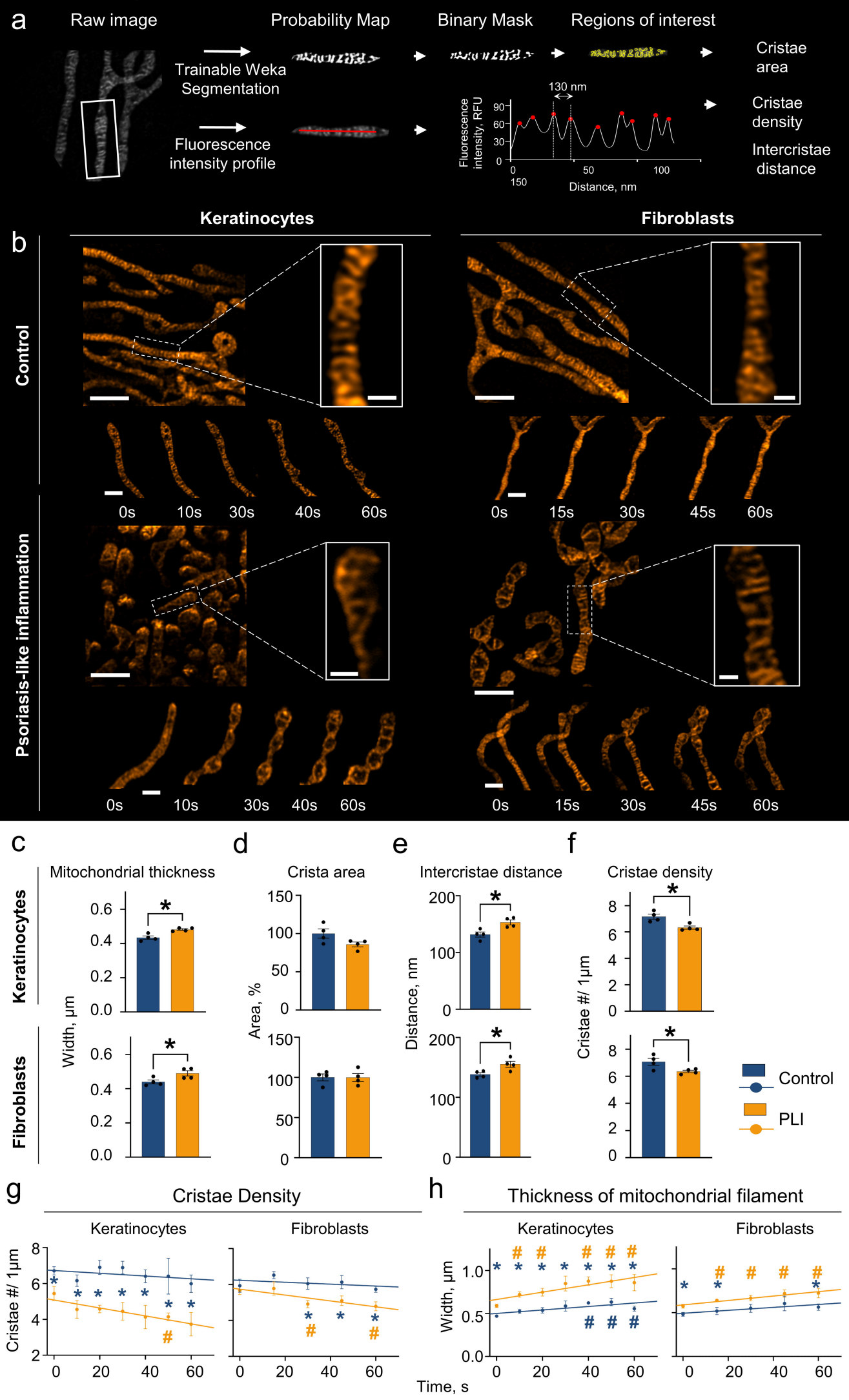
a
Raw image
Probability Map
Binary Mask
Regions of interest
Trainable Weka Segmentation
Fluorescence intensity profile
130 nm
Fluorescence intensity, RFU
Distance, nm
Cristae area
Cristae density
Intercristae distance
b
Keratinocytes
Fibroblasts
Control
Psoriasis-like inflammation
0s
10s
30s
40s
60s
15s
45s
c
Mitochondrial thickness
Width, µm
d
Crista area
Area, %
e
Intercristae distance
Distance, nm
f
Cristae density
Cristae #/ 1µm
Control
PLI
g
Cristae Density
Cristae #/ 1µm
h
Thickness of mitochondrial filament
Width, µm
Time, s

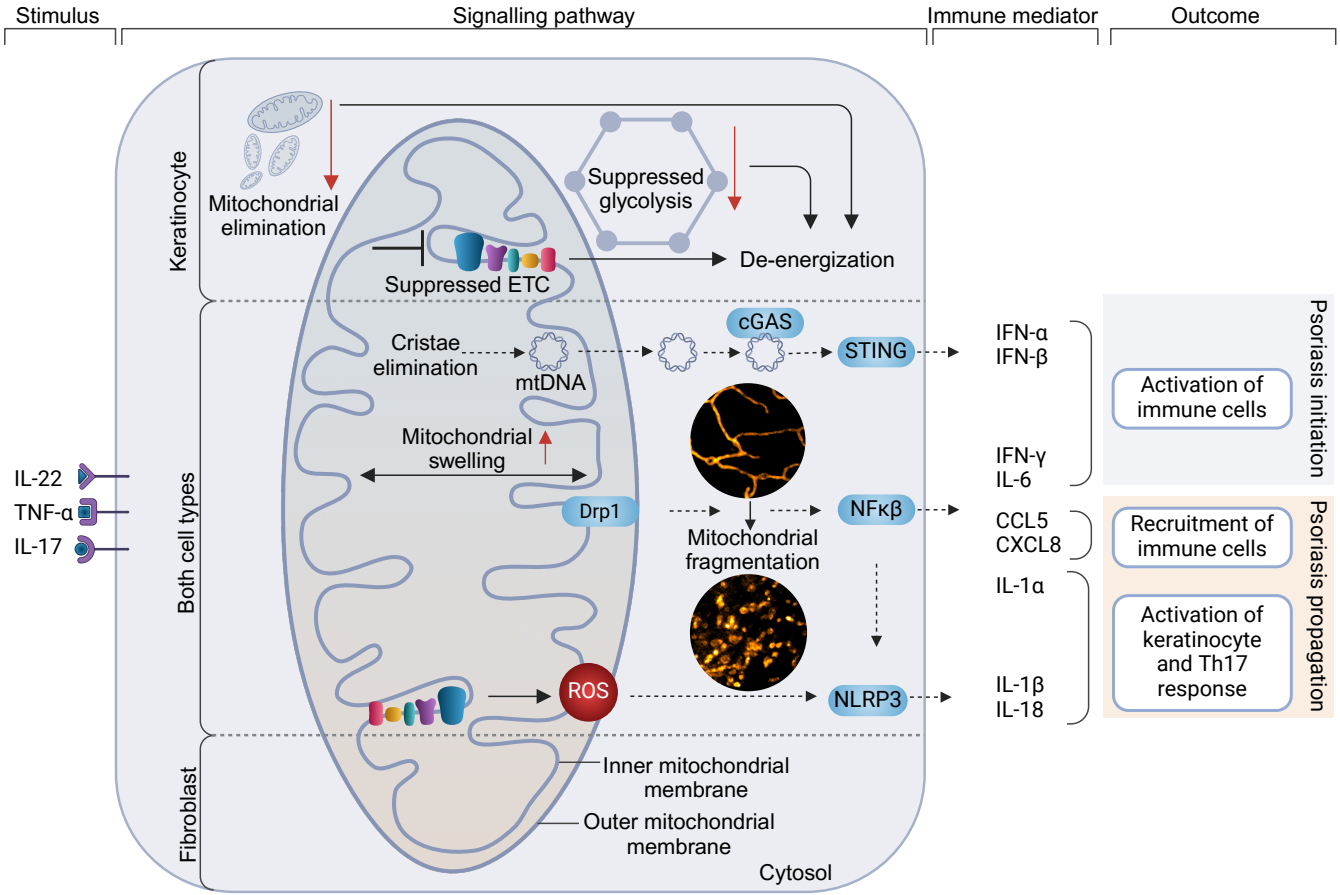
Stimulus
Signalling pathway
Immune mediator
Outcome
Keratinocyte
Both cell types
Fibroblast
Mitochondrial elimination
Suppressed glycolysis
Suppressed ETC
De-energization
Cristae elimination
mtDNA
cGAS
STING
Mitochondrial swelling
Drp1
Mitochondrial fragmentation
NFκβ
ROS
NLRP3
Inner mitochondrial membrane
Outer mitochondrial membrane
Cytosol
IL-22
TNF-α
IL-17
IFN-α
IFN-β
IFN-γ
IL-6
CCL5
CXCL8
IL-1α
IL-1β
IL-18
Activation of immune cells
Recruitment of immune cells
Activation of keratinocyte and Th17 response
Psoriasis initiation
Psoriasis propagation